Available online at www.sciencedirect.com
ScienceDirect
Journal of Magnetism and Magnetic Materials 305 (2006) 457–463
Journal of magnetism and magnetic materials
www.elsevier.com/locate/jmmm

The nature of charged zig-zag domains in MnAs thin films

R. Engel-Herbert[a], D.M. Schaadt[a], S. Cherifi[b,c], E. Bauer[b,d], R. Belkhou[e], A. Locatelli[b], S. Heun[b,f], A. Pavlovska[d], J. Mohanty[a], K.H. Ploog[a], T. Hesjedal[a,*,1]

[a]*Paul-Drude-Institut für Festkörperelektronik, Hausvogteiplatz 5–7, D-10117 Berlin, Germany*
[b]*Sincrotrone Trieste, S.S. 14, km 163.5, 34012 Basovizza (TS), Italy*
[c]*CNRS-Laboratoire Louis Néel, BP166 38042 Grenoble, France*
[d]*Department of Physics and Astronomy, Arizona State University, Tempe, AZ 85287-1504, USA*
[e]*LURE, Bat 209D, Université Paris-Sud, BP34 91898 Orsay, France*
[f]*Laboratorio Nazionale TASC, S.S. 14, km 163.5, Area Science Park, 34012 Basovizza (TS), Italy*

Received 9 August 2005; received in revised form 27 January 2006
Available online 6 March 2006

Abstract

We report on apparently charged domain walls in MnAs-on-GaAs(0 0 1) layers. For head-on domains, described as two domains facing each other with opposite magnetization, the domain walls of $\gtrsim$200 nm thick films exhibit a zig-zag pattern. Depending on the width of the ferromagnetic stripes, which is a function of temperature and thus the strain in the easy axis direction, the zig-zag angle 2θ increases from 90° in the case of wide stripes to 180° (i.e., to a straight wall) for narrow stripes. The underlying domain structure was calculated using a three-dimensional micromagnetic simulator. The calculations reveal a number of distinct domain patterns as a result of the system's attempt to reduce its energy through the formation of closure domain-like patterns in the easy plane. A diamond-like state consisting of two intersecting sub-surface domain walls is the underlying magnetic structure resulting in the observed, apparently charged domain walls. The zig-zag pattern of the domain boundary is explained by stray field minimization of the diamond state along the stripe.

PACS: 75.60.Ch; 75.70.Kw

Keywords: Magnetic domains; Magnetic thin films; Ferromagnet-semiconductor heterostructure; MnAs; X-ray magnetic circular dichroism; Photoemission electron microscopy

1. Introduction

Magnetic domains and the boundaries that separate them play a central role in magnetism [1]. Understanding and controlling domain patterns is important for many technological applications in spin electronics and enable possibilities for new devices [2]. Zig-zag domain boundaries between two regions of head-on magnetization (i.e., domains with opposite magnetization along the easy axis) occur in films with in-plane uniaxial anisotropy [1]. Their occurrence is connected with the reduction of magnetostatic energy and magnetic charge density through the increase of the effective wall length. Several systems exhibiting zig-zag walls, such as Gd–Co [3,4], permalloy [5], Co [6], and CoTi [7] have been investigated both experimentally and theoretically [4,7].

In this study, we report on apparently charged zig-zag domain walls in MnAs-on-GaAs(0 0 1) films. This material system allows a controlled variation of the width of the self-organized ferromagnetic stripes via the temperature [8–10]. Through investigations of samples with different thickness, the magnetic and the strain effects on the properties of such domain walls can be separated. Based on XMCDPEEM (X-ray magnetic circular dichroism photoemission electron microscopy) measurements, we present an analysis of the zig-zag angle, periodicity, and amplitude as a function of ferromagnetic stripe width and magnetic film thickness.

*Corresponding author. Tel.: +49 30 20377260; fax: +49 30 20377257.
E-mail address: hesjedal@pdi-berlin.de (T. Hesjedal).
[1]Permanent address: ECE Department, University of Waterloo, Canada.

0304-8853/$ - see front matter © 2006 Elsevier B.V. All rights reserved.
doi:10.1016/j.jmmm.2006.02.083

2. Experimental details

2.1. MnAs-on-GaAs(0 0 1)

The MnAs/GaAs(0 0 1) heterostructures were prepared as described in Ref. [14]. The preparation conditions assure that MnAs predominantly grows in the so-called A-orientation with MnAs($\bar{1}$ 1 0 0)‖GaAs(0 0 1) and MnAs[0 0 0 1] (*c*-axis) ‖GaAs[1 $\bar{1}$ 0]. In bulk MnAs, the ferromagnetic order discontinuously breaks down around 40 °C (α-MnAs → β-MnAs). In epitaxial MnAs films on GaAs(0 0 1), where the film is only free to expand perpendicular to the surface, a coupled first order magneto-structural phase transition is observed over a temperature range of 10–40 °C. The involved strain stabilizes an ordered stripe array of the two magnetically and structurally distinct phases extending along the *c*-axis [8–10].

The magnetic properties were investigated by SQUID (superconducting quantum interference device) magnetometry, and the domains were imaged at different temperatures by magnetic force microscopy (MFM) [11] and X-ray magnetic circular dichroism photoemission electron microscopy (XMCDPEEM) [12]. MnAs exhibits a magnetic easy plane perpendicular to the *c*-axis direction (which is the hard axis of magnetization) [13], however the shape anisotropy of the film leads to the formation of an easy axis of magnetization along the in-plane *a*-axis direction (along MnAs[1 1 $\bar{2}$ 0]) [14].

2.2. XMCDPEEM and LEEM measurements

The XMCDPEEM and LEEM (low energy electron microscopy) measurements of the MnAs/GaAs(0 0 1) samples were performed with an ELMITEC microscope at the 'Nanospectroscopy' undulator beamline at ELETTRA (Trieste, Italy). Secondary electrons produced in the photoionization of the Mn L_3 level were used for imaging. The samples were illuminated with the *a*-axis of MnAs in the plane of incidence of the light. In order to perform XMCDPEEM measurements on clean sample surfaces grown in Berlin, an As cap was deposited on top of MnAs before transport in a dry nitrogen atmosphere. After complete desorption of the As cap at about 300 °C in the preparation chamber at ELETTRA, low-energy electron diffraction of the MnAs ($\bar{1}$ 1 0 0) surface showed the (1 × 2) pattern which was also observed after growth, i.e. before capping the samples. The advantage of XMCDPEEM over MFM is the direct access to the magnetic domain structure. Whereas MFM images the stray field of the sample—sometimes even in an invasive way—surface-sensitive XMCDPEEM maps the magnetization component in the direction of the incident photon beam.

Fig. 1 shows a typical LEEM image of the topography (a) and XMCDPEEM image of the magnetic contrast (b), respectively. In the topography, the striped phase is clearly visible. The brighter stripes (α-phase) in the topographic image are ferromagnetic as identified in the magnetic image by the black and white areas, in which the direction of the magnetization and the incident light are antiparallel and parallel, respectively. The domain structure is typically classified by the number of stripe subdomains in the easy *a*-axis direction as types (I), (II) and (III) domains. In the figure, the dominating type (I) and (II) domains are labeled accordingly. As in thicker films, also type (III) domains are observed [15]. Moreover, tilted domain walls are found separating type (I) domains of opposite magnetization. The domain walls between type (II) domains, which run predominantly in the *c*-axis direction, exhibit a characteristic zig-zag pattern.

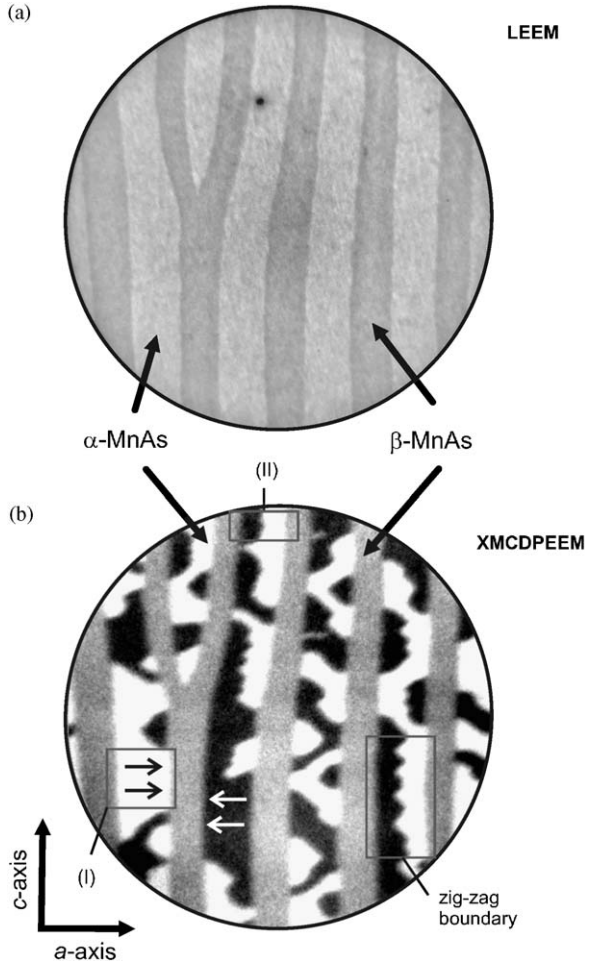

Fig. 1. Micromagnetic domain structure of a 500-nm-thick MnAs film on GaAs(0 0 1) determined using LEEM (a) and XMCDPEEM (b). In the LEEM image, the α–*β*-stripe structure is visible. The XMCDPEEM image shows the two basic domain types, labeled in the figure. The domain boundary of type (II) domains is also characterized by a zig-zag pattern. The field-of-view diameter is 10 μm.

3. Results

To study the nature of zig-zag domain walls in detail, we have investigated their occurrence and characteristics as a function of ferromagnetic stripe width and film thickness.

3.1. Thickness dependence of the magnetic domain structure

Fig. 2 shows three XMCDPEEM images obtained from MnAs films with a thickness of (a) 120 nm, (b) 215 nm, and (c) 300 nm. The ferromagnetic stripes can be identified as areas with black and white contrast. With increasing film thickness, the stripe period $p_{\alpha\beta}$ increases, where $p_{\alpha\beta}$ is defined as the sum of the α- and β-stripe widths w_α and w_β, respectively. From the analysis of a large number of samples, we found that $p_{\alpha\beta}$ is a linear function of the film thickness t with $p_{\alpha\beta} = 4.8 \cdot t$. The relative widths w_α and w_β, on the other hand, are also a function of temperature. The micromagnetic contrast for the 120-nm-thick film (Fig. 2(a)) is dominated by type (I) and (II) domains, whereas the thicker films show a significant number of type (III) domains as well. The domain boundaries between type (I) domains of opposite magnetization (running along the *a*-axis direction) show a large tilt for thin films and straight walls for thick films (cf., white circles in Fig. 2(a) and (b)). Type (II) domains are characterized by two oppositely magnetized head-on domains separated by a domain wall running along the *c*-axis direction. These walls are straight for the 120 nm thick film but they become increasingly textured in thicker films. The 300-nm-thick film exhibits fully developed zig-zag walls (cf., white rectangles in Fig. 2(a) and (c)). Type (III) domains are never observed below a critical film thickness of approximately 150 nm. In the 215-nm-thick film, extended type (III) domains show a zig-zag pattern along both domain boundaries (see rectangle in Fig. 2(b)). This has also been observed in the narrower stripes of the 300-nm-thick film. In contrast, wide ferromagnetic areas are characterized by tilted domain boundaries closer to the edges of the stripe and less extended type (III) domains.

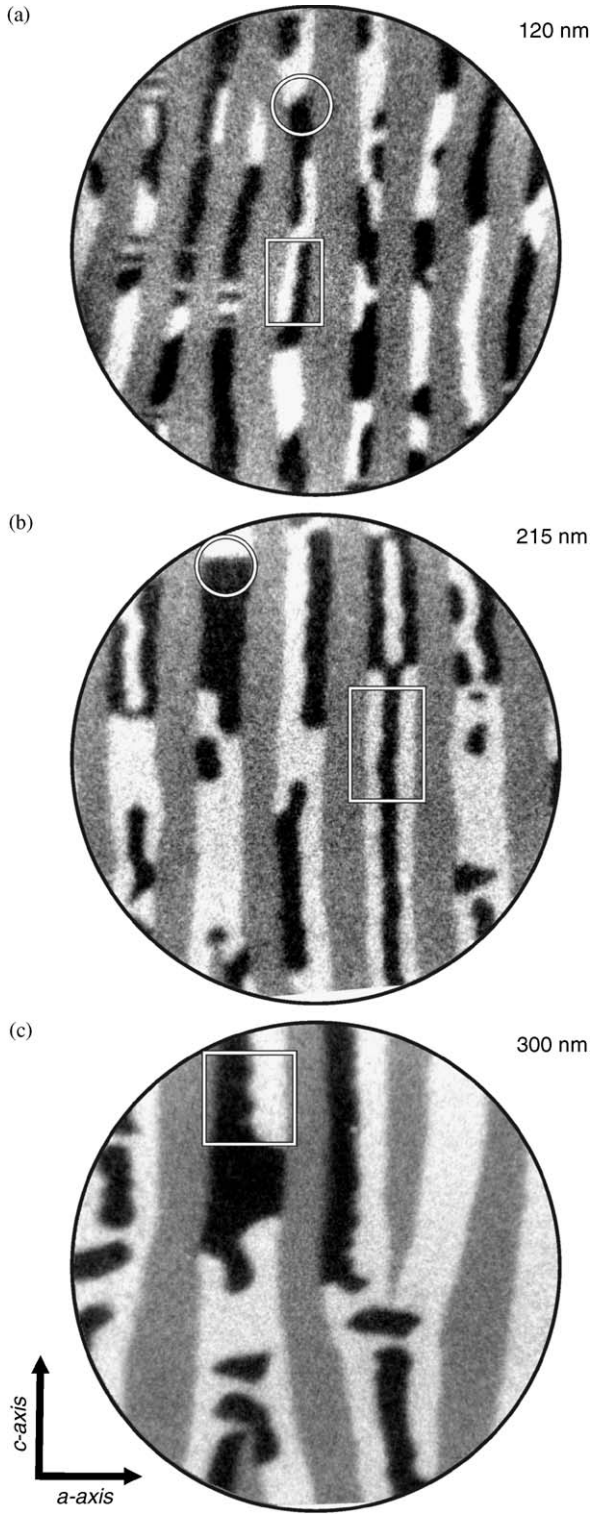

Fig. 2. Thickness dependence of the micromagnetic domain structure: (a) 120 nm, (b) 215 nm, and (c) 300 nm. The XMCDPEEM images were obtained at 20 °C. The field-of-view diameter is 5 μm.

3.2. Temperature dependence of the magnetic domain structure

To probe the dependence of the domain structure on the ferromagnetic stripe width, we performed temperature-dependent XMCDPEEM measurements on a 500-nm-thick film. As previously mentioned, thicker films exhibit a larger variety of domain structures, and the dynamics of many different structures can be observed simultaneously. Fig. 3 presents a selection of images obtained during a heating sequence. To obtain a magnetically well-defined state, the sample was cooled through the phase transition to a temperature well below 0 °C. In the complete α-phase, the sample shows no magnetic features on the probed length scale until β-MnAs dots start to form at a temperature of approximately 10 °C. At 22 °C, β-MnAs reorganizes and forms stripe segments before it finally exhibits a well-ordered stripe structure near 30 °C. The formation of regular structures occurs at lower temperatures in thinner films. With increasing separation of the ferromagnetic stripes, their demagnetization becomes energetically possible and occurs in thick films by flipping the middle part of a stripe (cf. lower part of Fig. 3(a)). The partial flipping of the stripe leads to a type (III) domain configuration with zig-zag domain boundaries near the edges of the stripe. At around 24 °C, the flipped areas separate and then start to extend along the stripe as the stripe narrows between 26

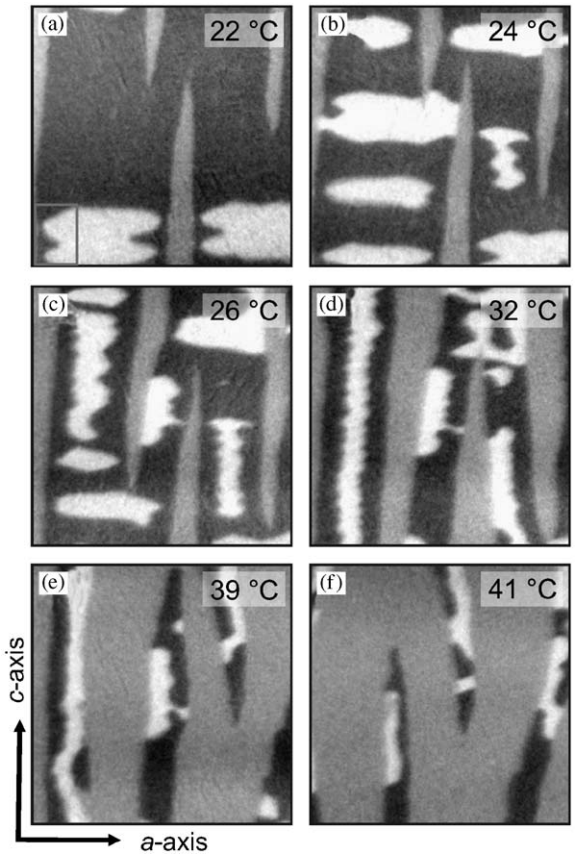

Fig. 3. Temperature dependence of the micromagnetic domain structure of a 500-nm-thick film: (a) 22 °C, (b) 24 °C, (c) 26 °C, (d) 32 °C, (e) 39 °C, and (f) 41 °C. The XMCDPEEM images measure $5 \times 5\,\mu m^2$.

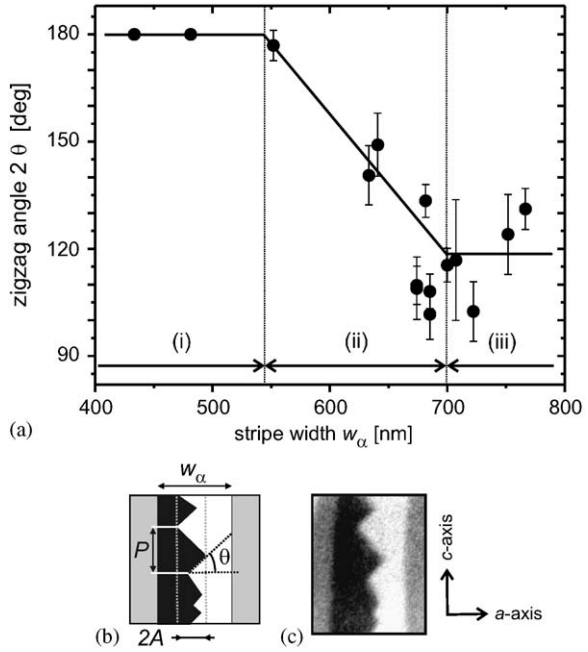

Fig. 4. (a) Plot of the zig-zag angle 2θ as a function of α-stripe width w_α for a 300-nm-thick film. Three regimes can be distinguished, as indicated in the graph. (b) Definition of the angle θ, the period P, and the amplitude $2A$ for a zig-zag wall (in a type (II) domain). (c) XMCDPEEM image of a zig-zag wall. The analyzed angles are indicated by black lines.

and 32 °C (cf. Fig. 3(c,d)). The extended type (III) domains show a zig-zag pattern of both domain boundaries, and the walls exhibit a partially correlated arrangement of the zig-zag angles. In the narrower parts of the ferromagnetic stripe network, only type (II) domains are found at 26 °C (cf. Fig. 3(c)). This trend continues until at approximately 35 °C at which point type (II) domains are predominant. At higher temperatures close to the phase transition temperature, the remaining stripe segments are primarily in a single domain state.

3.3. Zig-zag domain wall statistics

Thus far, we have only provided a qualitative description of the influence of the geometrical parameters, namely film thickness and ferromagnetic stripe width, on the micromagnetic domain pattern. We now present a statistical analysis of the zig-zag domain wall angle obtained from a number of measurements. For this purpose, we introduce the characteristic parameters of a zig-zag wall: the periodicity P, the angle 2θ, and the amplitude $2A$, as illustrated in Fig. 4(b).

From the analysis of type (II) zig-zag domains performed on a series of temperature-dependent XMCDPEEM images, we find (for a 300 and a 500-nm-thick film) the mean values for $2A$, P, the maximum α-stripe width up to which type (II) domains are observed $w_\alpha^{\max}$ (II), and the minimum α-stripe width down to which type (III) domains are still visible $w_\alpha^{\min}$ (III), as listed in Table 1. Type (I) domains exist under all conditions. For the 300 nm film, type (II) domains vanish as soon as type (III) domains nucleate. This does not imply that upon increasing the temperature suddenly only type (II) domains are found. In fact, the dynamic strain balance during the phase transition leads to a distribution of stripe widths w_α at a given temperature. For the 500 nm film, the remarkable finding is that between a α-stripe width of between 800 and 1000 nm neither type (II) nor type (III) domains are present. This is partially due to the formation of type (I) domains and to the fact that only a few segments of the stripes have a width in this range.

From the mean values of amplitude and period, one can calculate the average zig-zag angle using $\tan\theta = P/4A$, yielding $2\theta = 79^\circ$ for the 300-nm-thick film and 85° for the 500-nm-thick film. According to the model of Freiser [4], the ratio of the angles (in our case 0.93) should be the same as the ratio of the thicknesses (in our case 0.60), which is obviously not the case for the MnAs-on-GaAs system.

However, the situation becomes more complicated in MnAs than in Freiser's model due to the formation of a phase-separated stripe structure, in which the individual stripe geometry might affect the domain structure and thus the zig-zag angle statistics. Therefore, we analyzed the zig-zag angle as a function of α-stripe width for the 300-nm-thick film. Again, only type (II) domain boundaries were

Table 1
Mean values for the zig-zag amplitude $2A$, the period P, the ratio $2A/P$, the maximum α-stripe width up to which type (II) domains are observed $w_\alpha^{\max}$(II), and the minimum α-stripe width down to which type (III) domains are still visible $w_\alpha^{\min}$(III)

Thickness (nm)	$2A$ (nm)	P (nm)	$2A/P$	$w_\alpha^{\max}$(II) (nm)	$w_\alpha^{\min}$(III) (nm)
300	367	517	0.70	555	544
500	464	742	0.63	784	976

considered, as the formation of coupled zig-zags in type (III) domains further complicates the analysis (cf. Fig. 3(d) on the left-hand side). As particularly evident in the 500-nm-thick film, the formation of zig-zag type (III) domains proceeds via the coupling of both zig-zag domain boundaries, partially forming an elongated hexagonal structure.

Fig. 4(a) plots the zig-zag angle 2θ as a function of stripe width w_α. The stripe width was measured locally along with the angle for the complete set of data measured from 10 to 40 °C in steps of <1 °C. The data points correspond to the average angles and the error bars to the standard deviation. The plot of the zig-zag angle exhibits three distinct regimes. In regime (i), below a critical stripe width of 540 nm, a constant angle of 180° is found, i.e. a straight domain wall. Straight walls are also characteristic for films thinner than 150 nm (not shown)—independent of w_α. Contrary to that, the 500-nm-thick film (not shown) exhibits a straight domain wall only for very narrow stripes ($w_\alpha < 250$ nm). In the intermediate regime (ii) from 540 to 700 nm the zig-zag angle decreases linearly with increasing stripe width. Regime (iii) is again exhibiting a constant angle, however, being approximately 115° for $w_\alpha > 700$ nm. For thicker films, the lower limit for 2θ is 90° and it is observed for α-stripes wider than 725 nm.

It is now interesting to focus on the stripe width below which the domain boundaries straighten, i.e. when the zig-zag boundaries are no longer energetically advantageous for the system. We find $w_\alpha = 540$ nm for the 300-nm-thick film and $w_\alpha = 250$ nm for the 500-nm-thick film, i.e. geometrical ratios of $w_\alpha/t = 1.8$ and 0.5, respectively. This finding excludes the possibility that the geometrical ratio, and thus the shape anisotropy, is the governing factor for the observed zig-zag wall behavior because, if it was, one should find a critical ratio $(w_\alpha/t)_{\text{crit}}$ which is universal for the material system [4].

4. Discussion

Before we thoroughly discuss our results concerning the zig-zag domains, we will revisit one common model for the formation of zig-zag domain walls [4]. A prerequisite for the appearance of zig-zag domain walls is certainly charged domain walls. Magnetic charges are a result of different normal components of the magnetization on both sides of the wall. Charged walls are most likely to occur in samples with low saturation magnetization or very thin films, as charges dramatically increase the magnetostatic energy. For the MnAs-on-GaAs system, we find head-to-head domains, which are also well-known from Gd–Co films [3]. As the direction perpendicular to the easy in-plane a-axis along the stripes is the hard axis of magnetization, the magnetization vector can hardly rotate out of the a-axis direction in the film plane. Furthermore, as no anisotropy associated with the deviation of the magnetization direction from the easy axis direction has to be taken into account, the nucleation of a zig-zag-shaped wall reduces the charge density per domain length. According to the model of Freiser [4], the zig-zag angle is inversely proportional to the film thickness t with the proportionality constant being determined by the exchange constant and the saturation magnetization. The zig-zag amplitude $2A$ scales with film thickness as t^3. As described above, we do not observe these proportionalities in MnAs. Moreover, the domain wall angle is not a result of the shape anisotropy, as we should observe the same angle for identical α-stripe width-to-thickness ratios w_α/t.

In the following, we discuss the possible origin of zig-zag domain boundaries. We start with a closer look at the most simple domain configuration in MnAs showing zig-zag domain boundaries, i.e., type (II) domains.

4.1. The nature of 'charged' domain walls in MnAs-on-GaAs

From XMCDPEEM measurements, which yield the magnetization of the surface layers of the sample, the observed head-to-head domains—termed type (II) domains—are fairly difficult to understand in the context of micromagnetics. In MFM measurements type (II) domains are easily identified [15]. The magnetization distribution deduced from the measurement of the out-of-plane component of the stray field, namely that of two oppositely magnetized bar magnets, supports at first sight the simple picture of a type (II) domain. However, the width of the domain wall separating the two oppositely magnetized subdomains of a type (II) domain seems broadened [16]. This observation, and the fact that the domain configuration assuming head-to-head bar magnets is energetically so unfavorable, stimulated three-dimensional simulations of the domain structure of MnAs [17].

The simulations were performed on a parallel micromagnetic simulator [18] based on OOMMF [19] assuming the following values for the magnetic parameters of MnAs: exchange stiffness constant $A = 1 \times 10^{-11}$ J/m and saturation magnetization $M_s = 4 \times 10^5$ A/m. In hexagonal crystals, the anisotropy energy is solely a function of the angle Θ between the magnetization $\mathbf{m}$ and the c-axis: $\varepsilon_{\text{ani}} = -K_{u_1} \sin^2\Theta - K_{u_2} \cos^4\Theta + \cdots$, where odd powers vanish for symmetry reasons. Crystals with an easy plane perpendicular to the anisotropy axis, i.e. the c-axis, are described by $K_{u_1}, K_{u_2} < 0$. The second order anisotropy constant at room temperature was determined by SQUID

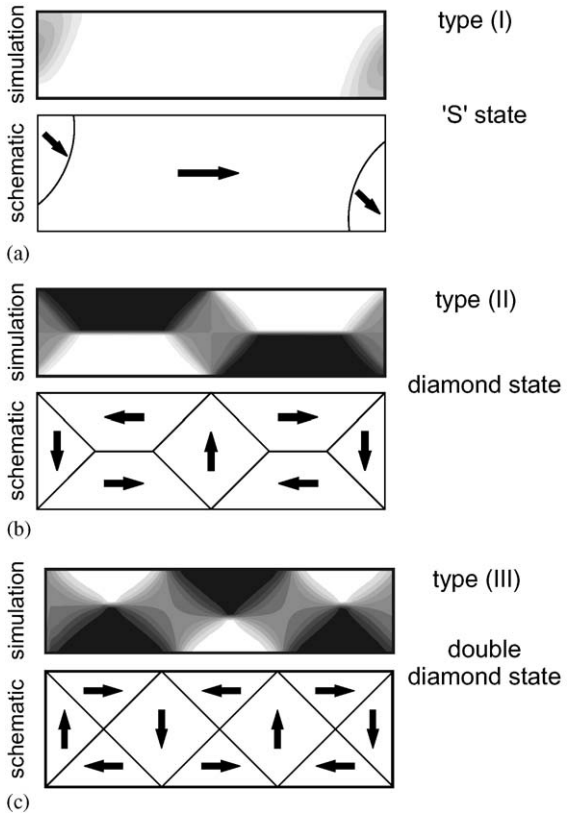

Fig. 5. Cross-sections of simulated domain configurations in the easy plane of MnAs films (above) and a schematic representation of the magnetization distribution (below). The 'S' state which leads to the observed type (I) domains is shown in (a), and the single and double diamond states leading to type (II) and (III) domains are given in (b) and (c), respectively. The diamond state domain structure clearly shows that MnAs does not exhibit charged domain walls.

magnetometry [14] and ferromagnetic resonance spectroscopy [20] to be $K_{u_1} = -7.2 \times 10^5\,\mathrm{J/m^3}$. The negative sign of K_{u_1} reflects the fact that the magnetization in MnAs prefers the basal plane. The fourth order anisotropy constant, which is in most cases negligible, was chosen to be $K_{u_2} = -3.6 \times 10^5\,\mathrm{J/m^3}$.

The simulation grid was chosen such that the cell dimensions (3 nm) are smaller than both the magnetocrystalline and the magnetostatic exchange lengths. The simulated domain states are not only a function of the geometrical ratio α-stripe width-to-thickness of the film w_α/t, but also of the absolute dimensions. In general, domain walls are energetically less favored in smaller structures, i.e. thinner films [17].

The simulations exhibit the same surface magnetization as observed in XMCDPEEM measurements and thus confirm our general domain classification scheme [16]. However, as MnAs exhibits an easy plane of magnetization perpendicular to the surface [13], the formation of a truly three-dimensional magnetization distribution is key to understanding the domain patterns in MnAs.

Fig. 5 shows cross-sectional cuts through the three-dimensional magnetization patterns along the easy *a*-axis direction in selected areas. For clarity, the schematics (Fig. 5(a)–(c)) indicate the magnetization directions from the calculated distributions (above). The three patterns that lead to the classified domains (I–III), namely the 'S' state, the diamond state, and the double diamond state, are depicted in (a–c), respectively. In case of a type (I) domain, the simple picture of a homogeneously magnetized bar magnet is altered by slightly tilted edges that only slightly influence the surface magnetization. In MFM, the 'S' state leads to a contrast enhancement of the features expected from an ideal bar magnet and are therefore hard to distinguish. The magnetization pattern which is responsible for the observed type (II) structure is, in fact, a diamond-shaped domain state, meaning that the 'charged' walls visible at the surface are actually intersections of two subsurface domain walls where the magnetization rotates by 90°. Type (III) domains, on the other hand, turn out to be made up of two diamond states. In this context, it is easy to understand that type (III) domains need a critical stripe width in order to be able to nucleate two diamonds. In addition, type (III) domains are energetically preferred over type (II) domains in wider stripes as the stray field is further reduced.

4.2. Why are there zig-zag domains in MnAs thin films?

Considering the three-dimensional magnetization pattern that is the basis of a type (II) domain, the previously discussed models for the formation of zig-zag domains are too simplistic. For instance, the sheer reduction of the charge density per domain length in the *c*-axis direction cannot account for the zig-zag domains. In the following discussion, we propose a model for the formation of zig-zag boundaries. We restrict ourselves to single zig-zag domains, i.e. type (II) domains, as zig-zag patterns in type (III) domains couple across the stripe which further complicates the situation. Double zig-zag walls are, however, well-known in magnetostatically coupled permalloy bilayers [21]. A model of the zig-zag domain wall in MnAs is shown in Fig. 6(a).

Focusing first on the nucleation of zig-zag boundaries, the onset of domain formation in previously single-domain areas is visualized in the temperature-dependent measurements of a 500-nm-thick film (cf. rectangle in Fig. 3(a)). Simulations have shown that type (I) domains are in fact the result of an 'S'-shaped state with deformed edges (cf. Fig. 5(a)). As soon as β-MnAs stripes nucleate in the previously homogeneous α-phase, 'S' states form where the magnetization at the edges is predominantly out-of-plane. To minimize the stray field, trapezoidal closure domain-like structures with an in-plane magnetization are formed [17]. In areas that are about to become type (III) domains, the alternating trapezoidal closure domains on both sides of the stripe are correlated. This state can be simulated by looking at very thick samples with a narrow α-stripe width such that a diamond state cannot nucleate. The result of the simulation is shown in Fig. 6(b). The fact that the

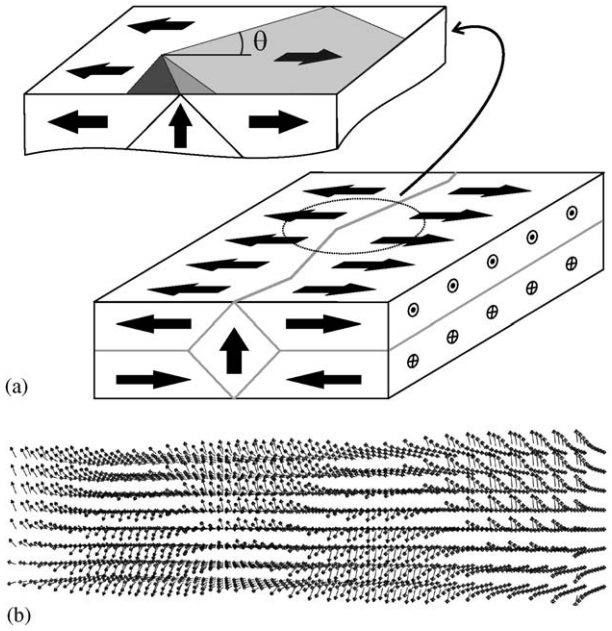

Fig. 6. (a) Model of a zig-zag domain wall in MnAs films. The underlying domain structure shows a diamond state, i.e. the apparently charged domain walls are actually intersections of two sub-surface walls. The close-up illustrates the zig-zag angle and tilt of the diamond state. (b) Plan view of the simulated magnetization distribution indicating the micromagnetic nature of the zig-zag domain wall structure in MnAs.

periodically deformed edge state can be simulated in a straightforward manner leads to the conclusion that the formation of zig-zag domain boundaries is a consequence of the stray field minimization.

The further process of zig-zag boundary formation away from the stripe edges proceeds by the inward growth of the trapezoidal closure domains with decreasing α-stripe width, until they meet in the middle of the stripe. Then, the resulting elongated, diamond-shaped domains separate (cf. Fig. 3(b), bottom left corner). As the β-MnAs organize into stripes, the central part of the stripe entirely flips its magnetization [type (II) → type (III)] and the zig-zag boundaries nucleate from the initial trapezoidal edge domains. A complete simulation of the nucleation process is not feasible, as in real films additional unknown physical boundary conditions have to be taken into account, such as pinning, which further determine the exact location of the edge domains and therefore the exact local zig-zag angle and period.

In summary, the driving mechanism of the zig-zag formation in MnAs is the minimization of the stray field of a diamond state. In the future, simulations on a larger volume will be performed to precisely describe the zig-zag state and to study the influence of the sample geometry.

5. Conclusions

In conclusion, we presented an analysis of zig-zag domain walls in MnAs. Depending on film thickness and temperature, and thus on the ferromagnetic stripe width, zig-zag angles 2θ between 90° for thick films and wide stripes and straight walls ($2\theta = 180°$) for thin films and narrow stripes are found. The simulated three-dimensional magnetization patterns reveal that the observed head-to-head or type (II) domains are due to a diamond state in depth. The domain boundary starts exhibiting a zig-zag pattern as the stripes widen, driven by a stray field minimization along the stripe.

Acknowledgements

The authors thank J. A. H. Stotz for valuable discussions, C. Herrmann and the Nanostructuring department for the sample preparation and acknowledge support by ELETTRA, the EU under contract HPRI-CT-1999-00033, and the BMBF (Germany). E. B. acknowledges support of this work by the NSF under Grant no. 9818296 and by the ONR Grant no. N-000140210922.

References

[1] A. Hubert, R. Schäfer, Magnetic Domains: The Analysis of Magnetic Microstructures, Springer, Berlin, 1998.
[2] J. Ferré, Topics Appl. Phys. 83 (2002) 127165.
[3] R.C. Taylor, A. Gangulee, J. Appl. Phys. 47 (1976) 4666.
[4] M.J. Freiser, IBM J. Res. Dev. 23 (1979) 330.
[5] E.J. Hsieh, R.F. Soohoo, AIP Conf. Proc. 5 (1971) 727.
[6] D.D. Dressler, J.H. Judy, IEEE Trans. Magn. MAG-10 (1974) 674.
[7] S. Hamzaoui, M. Labrune, I.B. Puchalska, Appl. Phys. Lett. 45 (1984) 1246.
[8] L. Däweritz, F. Schippan, M. Kästner, B. Jenichen, V.M. Kaganer, K.H. Ploog, B. Dennis, K.-U. Neumann, K.R.A. Ziebeck, Proceedings of the 28th International Symposium Compound Semiconductors, IOP Conference Series No. 170, vol. 269, IOP, Bristol, 2002.
[9] T. Plake, M. Ramsteiner, V.M. Kaganer, B. Jenichen, M. Kästner, L. Däweritz, K.H. Ploog, Appl. Phys. Lett. 80 (2002) 2523.
[10] V.M. Kaganer, B. Jenichen, F. Schippan, W. Braun, L. Däweritz, K.H. Ploog, Phys. Rev. B 66 (2002) 045305.
[11] T. Plake, T. Hesjedal, J. Mohanty, M. Kästner, L. Däweritz, K.H. Ploog, Appl. Phys. Lett. 82 (2003) 2308.
[12] E. Bauer, S. Cherifi, L. Daeweritz, M. Kaestner, S. Heun, A. Locatelli, J. Vac. Sci. Technol. B 20 (2002) 2539.
[13] R.W. De Blois, D.S. Rodbell, Phys. Rev. 130 (1963) 1347.
[14] F. Schippan, G. Behme, L. Däweritz, K.H. Ploog, B. Dennis, K.-U. Neumann, K.R.A. Ziebeck, J. Appl. Phys. 88 (2000) 2766.
[15] R. Engel-Herbert, J. Mohanty, A. Ney, T. Hesjedal, L. Däweritz, K.H. Ploog, Appl. Phys. Lett. 84 (2004) 1132.
[16] R. Engel-Herbert, T. Hesjedal, D. Schaadt, J. Mohanty, L. Däweritz, K.H. Ploog, E. Bauer, A. Pavlovska, S. Cheri, A. Locatelli, S. Heun, unpublished.
[17] R. Engel-Herbert, T. Hesjedal, D. Schaadt, unpublished.
[18] D.M. Schaadt, MMF—three-dimensional parallel micromagnetic simulator, unpublished.
[19] M. Donahue, D. Porter, http://math.nist.gov/oommf.
[20] J. Lindner, T. Toliński, K. Lenz, E. Kosubek, H. Wende, A. Baberschke, A. Ney, T. Hesjedal, C. Pampuch, R. Koch, L. Däweritz, K.H. Ploog, J. Magn. Magn. Mat. 277 (1–2) (2004) 159.
[21] L.A. Finzi, J.A. Hartmann, IEEE Trans. Magn. MAG-4 (1968) 662.